

Fast Nonlinear Fourier Transform Algorithms Using Higher Order Exponential Integrators

Shrinivas Chimmalgi, Peter J. Prins and Sander Wahls, *Senior Member, IEEE*

Abstract—The nonlinear Fourier transform (NFT) has recently gained significant attention in fiber optic communications and other engineering fields. Although several numerical algorithms for computing the NFT have been published, the design of highly accurate low-complexity algorithms remains a challenge. In this paper, we present new fast NFT algorithms that achieve accuracies that are orders of magnitudes better than current methods, at comparable run times and even for moderate sampling intervals. The new algorithms are compared to existing solutions in multiple, extensive numerical examples.

Index Terms—Nonlinear Fourier Transform, Transforms for signal processing, Fast algorithms for DSP, Nonlinear signal processing.

I. INTRODUCTION

THE fast Fourier transform (FFT) is a well-known success story in engineering. From a numerical point of view, this is quite surprising since, at first sight, the FFT provides a mere first-order approximation of the discrete-time Fourier transform one is actually interested in. Upon closer inspection, it however turns out that approximations based on FFTs perform much better once the underlying signal is smooth [17]. Recently, *nonlinear* Fourier transforms (NFTs) have been gaining much attention in engineering areas such as fiber-optic communications [3], [35] and coastal engineering [12], [24]. NFTs are generalizations of the conventional Fourier transform that allow to solve specific nonlinear evolution equations in a way that is analog to how Fourier solved the heat equation [1]. The evolution of the nonlinear Fourier spectrum is, exactly like in the linear case, much simpler than the evolution of the original signal. NFTs also have unique data analysis capabilities that enable the detection of particle-like signal components known as solitons [31]. Recently, a nonlinear variant of the FFT has been derived [41], [42]. These type of fast NFTs (FNFTs) can provide up to second-order accuracy [35]. Unfortunately, unlike for the FFT, the accuracy of the FNFTs in [35], [41], [42] remains (at most) second-order even if the underlying signal is smooth. As a result, engineers currently have to strongly oversample even smooth signals in order to get reliable numerical results ([16, Sec. 4]). Several authors have proposed NFT algorithms with higher orders of accuracy, utilizing either Runge-Kutta [13], [45] or implicit

Adams methods [36]. However, even though these methods have higher accuracy orders, they require very small sampling intervals in order to actually perform better than standard second-order methods such as [10]. For practically relevant sampling intervals, they are typically not the best choice as they are slower *and* may even perform worse in these regimes. Numerical methods that provide better complexity-accuracy trade-offs in practically relevant regimes have been an open problem until recently. In [14], the authors introduced a new numerical method that can compute the NFT with accuracies that are orders of magnitudes better than those of standard methods while having comparable run times. In this paper, the following three contributions are made.

- 1) Improved variants of the numerical NFT in [14] with even better complexity-accuracy trade-offs are presented and investigated in detailed numerical examples.
- 2) Fast versions of the new numerical NFTs are derived.
- 3) A series acceleration technique is investigated to improve the complexity-accuracy trade-off even further.

To give an illustration of the achieved gains, we point out that in one of our numerical examples, the best-performing of our new methods achieves an accuracy that is *hundred million* times better than the standard second-order method in [10] at a comparable run time.¹

The paper is structured as follows. In Sec. II, we derive improved versions of our recently proposed numerical NFT in [14], and compare them with both conventional second-order and other higher-order NFT algorithms in multiple numerical examples. Then, in Sec. III, we demonstrate how some of our new numerical NFTs can be made fast. The fast versions are compared with their slow counterparts. Next, in Sec. IV, we investigate how series acceleration techniques can improve the complexity-accuracy trade-off of the fast NFT methods even further. Sec. V deals with a special part of the NFT that occurs only in some cases. The paper is finally concluded in Sec. VI.

Notation

Real numbers: \mathbb{R} ; $\mathbb{R}_{\geq 0} := \{x \in \mathbb{R} : x \geq 0\}$; Complex numbers: \mathbb{C} ; Complex numbers with positive imaginary part: \mathbb{H} ; Integers: \mathbb{Z} ; $i := \sqrt{-1}$; Euler's number: e ; Real part: $\text{Re}(\cdot)$; Complex conjugate: $(\cdot)^*$; Floor function: $\lfloor \cdot \rfloor$; Absolute value: $|\cdot|$; Matrix exponential: $\text{expm}(\cdot)$; Matrix product: $\prod_{k=1}^K A_k := A_K A_{K-1} \times \dots \times A_1$; Matrix element in the i th

All authors are with the Delft Center for Systems and Control, Delft University of Technology, Mekelweg 2, 2628 CD Delft, The Netherlands. E-mail: s.chimmalgi@tudelft.nl.

Some of the results were presented at the OSA Advanced Photonics Congress, Zurich, July 2018 (SpM4G.5)

This project has received funding from the European Research Council (ERC) under the European Unions Horizon 2020 research and innovation programme (grant agreement No 716669).

¹Compare the error for $\text{CF}_1^{[2]}$ in Fig. 6 with that of $\text{FCF_RE}_2^{[4]}$ in Fig. 13 for the execution time 1 sec. We remark that although the execution times are implementation specific, they still give a good indication of the advantages our proposed algorithm.

column and j th row: $[\cdot]_{i,j}$; Fourier transform of function $f(t)$, $\tilde{f}(\xi) = \int_{-\infty}^{\infty} f(t)e^{-it\xi} dt : \mathcal{F}(f(t))$; Inverse Fourier transform of function $\tilde{f}(\xi)$, $f(t) = \frac{1}{2\pi} \int_{-\infty}^{\infty} \tilde{f}(\xi)e^{it\xi} d\xi : \mathcal{F}^{-1}(\tilde{f}(\xi))$.

A. Nonlinear Fourier Transform (NFT)

In this section we describe the mathematical machinery beyond the NFT. Let $q(x, t)$ denote the complex envelope of the electric field in an ideal optical fiber, whose evolution in normalized coordinates is described by the nonlinear Schrödinger equation (NSE) [2, Chap. 2]

$$i\frac{\partial q}{\partial x} + \frac{\partial^2 q}{\partial t^2} + 2\kappa|q|^2q = 0. \quad (1)$$

Here, $x \geq 0$ denotes the location in the fiber and t denotes retarded time. The parameter κ determines if the dispersion in the fiber is normal (-1) or anomalous (+1). When $\kappa = +1$ Eq. 1 is referred to as the focusing NSE and for $\kappa = -1$ as the defocusing NSE. The NFT that solves the NSE (Eq. 1) is due to Zakharov and Shabat [46]. It transforms any signal that vanishes sufficiently fast for $t \rightarrow \pm\infty$ from the time-domain to the nonlinear Fourier domain through the analysis of the linear ordinary differential equation (ODE)

$$V_t(t, \lambda) = C(t, \lambda)V(t, \lambda) = \begin{bmatrix} -i\lambda & q(t) \\ -\kappa q^*(t) & i\lambda \end{bmatrix} V(t, \lambda), \quad (2)$$

where $q(t) = q(0, t)$, subject to the boundary conditions

$$\begin{aligned} \lim_{t \rightarrow -\infty} V(t, \lambda) &= \begin{bmatrix} \phi(t, \lambda) & \bar{\phi}(t, \lambda) \end{bmatrix} \rightarrow \begin{bmatrix} e^{-i\lambda t} & 0 \\ 0 & -e^{i\lambda t} \end{bmatrix}, \\ \lim_{t \rightarrow \infty} V(t, \lambda) &= \begin{bmatrix} \psi(t, \lambda) & \bar{\psi}(t, \lambda) \end{bmatrix} \rightarrow \begin{bmatrix} 0 & e^{-i\lambda t} \\ e^{i\lambda t} & 0 \end{bmatrix}. \end{aligned} \quad (3)$$

The term $\lambda \in \mathbb{C}$ is a spectral parameter similar to s in the Laplace domain. The matrix $V(t, \lambda)$ is said to contain the eigenfunctions since Eq. 2 can be rearranged into an eigenvalue equation with respect to λ [1]. One can view the eigenfunctions $V(t, \lambda)$ as being scattered by $q(t)$ as they move from $t \rightarrow -\infty$ to $t \rightarrow \infty$. Hence Eq. 2 is referred to as the scattering problem [46]. (Many problems in signal processing can be expressed through such scattering problems [11].) For Eq. 2 subject to boundary conditions Eq. 3, there exists a unique matrix called the scattering matrix

$$\mathcal{S}(\lambda) = \begin{bmatrix} a(\lambda) & \bar{b}(\lambda) \\ b(\lambda) & -\bar{a}(\lambda) \end{bmatrix}, \quad (4)$$

such that [1]

$$\begin{bmatrix} \phi(t, \lambda) & \bar{\phi}(t, \lambda) \end{bmatrix} = \begin{bmatrix} \bar{\psi}(t, \lambda) & \psi(t, \lambda) \end{bmatrix} \mathcal{S}(\lambda). \quad (5)$$

The components $a(\lambda)$, $b(\lambda)$, $\bar{b}(\lambda)$ and $\bar{a}(\lambda)$ are known as the scattering data. The components $a(\lambda)$ and $b(\lambda)$ are sufficient to describe the signal completely. Their evolution along the x dimension (along the length of the fiber) is simple [1, Sec. III]

$$\begin{aligned} a(x, \lambda) &= a(0, \lambda), \\ b(x, \lambda) &= b(0, \lambda)e^{-4i\lambda^2 x}. \end{aligned} \quad (6)$$

The *reflection coefficient* is then defined as $\rho(\lambda) = b(\lambda)/a(\lambda)$ for $\lambda \in \mathbb{R}$. The nonlinear Fourier spectrum can also contain a so-called *discrete spectrum* in the case of $\kappa = 1$. It

corresponds to the complex poles of the reflection coefficient in the upper half-plane, which are given by the zeros $\lambda_k \in \mathbb{H}$ of $a(\lambda)$. It is known that there are only finitely many (N) such poles. The poles λ_k are also referred to as eigenvalues and a corresponding set of values $b_k := b(\lambda_k)$ are known as norming constants. There are different ways to define a nonlinear Fourier spectrum. One possibility is $\{\rho(\lambda)\}_{\lambda \in \mathbb{R}}$, $(\lambda_k, \rho_k := b_k / \frac{\partial a(\lambda)}{\partial \lambda})_{k=1}^N$ [1]. The other is $\{b(\lambda)\}_{\lambda \in \mathbb{R}}$, $(\lambda_k, b_k)_{k=1}^N$ [18]. In this paper we are primarily interested in computation of $\rho(\lambda)$ but some notes regarding computation of $b(\lambda)$ and the λ_k will also be given. Although we will illustrate our algorithms by applying them to the specific case of NFT of NSE with vanishing boundary condition, it should be noted that we are primarily presenting algorithms for solving equations similar to Eq. 2 [1, Eq. 2]. Hence the algorithms presented in this paper can be extended to compute the NFTs w.r.t to other nonlinear evolution equations such as the Korteweg-de Vries equation [26].

II. NUMERICAL COMPUTATION OF NFT USING HIGHER ORDER EXPONENTIAL INTEGRATORS

In this section we will start by outlining some assumptions required for the numerical methods that will be presented. We will give a brief overview of one of the approaches for computing the NFT and then talk specifically about our proposal to use a special class of so-called exponential integrators. To evaluate the methods, we describe examples and performance criteria. We will finally show and compare the results for various methods applied to the mentioned examples.

A. Assumptions

The numerical computation of the NFT is carried out with discrete data samples on finite precision machines. Hence, we need to make the following assumptions:

- 1) The support of the potential $q(t)$ is truncated to a finite interval, $t \in [T_-, T_+]$, instead of $t \in (-\infty, \infty)$. The values T_{\pm} are chosen such that the resulting truncation error is sufficiently small. The approximation is exact if $q(t) = 0 \forall t \notin [T_-, T_+]$.
- 2) The interval $[T_-, T_+]$ is divided into D subintervals of width $h = (T_+ - T_-)/D$. We assume that the signal is sampled at the midpoints of each subinterval $t_n = T_- + (n + 0.5)h$, $n = 0, 1, \dots, D-1$ such that $q_n := q(t_n)$.

B. Numerical Scattering

The main step in numerically computing the NFT is to solve the scattering problem in Eq. 2 for $\phi(T_+, \lambda)$ for different values of λ . We can view the D subintervals as layers which scatter the eigenfunction $\phi(t, \lambda)$ as it moves from $t = T_-$ to $t = T_+$. Using numerical ODE solvers we solve for an approximation $\hat{\phi}(T_+, \lambda)$ of $\phi(T_+, \lambda)$. By taking $\psi(T_+, \lambda)$ equal to the limit in Eq. 3 at $t = T_+$, we can compute a numerical approximation of the scattering data and ultimately the reflection coefficient.

C. Exponential Integrators

Almost any numerical method available in literature for solving ODEs can be used to solve for $\phi(T_+, \lambda)$ [13], [37]. However, we are particularly interested in so-called exponential type integrators. These methods have been shown to provide a very good trade-off between accuracy and computational cost in several numerical benchmark problems while being fairly easy to implement, see [7] and references therein. We propose to use a special sub-class known as commutator-free quasi-Magnus (CFQM) exponential integrators as some NFT algorithms based on these integrators turn out to have the special structure [41] that is needed to make them fast. We show this in Sec. III.

For rest of the paper we adopt the notation used in [8]. The results in [8] provide the following iterative scheme to compute a numerical approximation $\hat{\phi}(T_+, \lambda)$ of $\phi(T_+, \lambda)$:

$$\begin{aligned}\hat{\phi}_{n+1}(\lambda) &= \text{CF}_J^{[r]}(t_n, \lambda) \phi_n(\lambda) = \prod_{j=1}^J e^{B_j(t_n, \lambda)} \phi(t_n, \lambda) \\ &= e^{B_J(t_n, \lambda)} \dots e^{B_1(t_n, \lambda)} \phi_n(\lambda) \\ &= \phi(t_{n+1}, \lambda) + \mathcal{O}(h^{r+1}),\end{aligned}\quad (7)$$

where

$$\begin{aligned}B_j(t_n, \lambda) &= h \sum_{k=1}^K a_{jk} C_k(t_n, \lambda), \quad j \in \{1, \dots, J\}, \\ C_k(t_n, \lambda) &= C(t_n + (c_k - 0.5)h), c_k \in [0, 1], k \in \{1, \dots, K\}.\end{aligned}\quad (8)$$

By iterating from $n = 0, 1, \dots, D-1$, we obtain the numerical approximation of $\phi(T_+, \lambda)$ that we need to compute the NFT. Denoting $\text{CF}_J^{[r]}(t_n, \lambda)$ in short by $G_n(\lambda)$ we can write

$$\begin{aligned}\hat{\phi}(T_+, \lambda) &= G_{D-1}(\lambda) G_{D-2}(\lambda) \dots G_0(\lambda) \phi(T_-, \lambda) \\ &= \prod_{n=0}^{D-1} G_n(\lambda) \phi(T_-, \lambda) = H(\lambda) \phi(T_-, \lambda).\end{aligned}\quad (9)$$

For an integrator $\text{CF}_J^{[r]}$, r is the order and J is the number of matrix exponentials required for each subinterval. An integrator of order r has local error (error in each subinterval) of $\mathcal{O}(h^{r+1})$. Over $D \propto 1/h$ such subintervals i.e., over the interval $[T_-, T_+]$, the global error will be $\mathcal{O}(h^r)$. This distinction of local and global error will become important when we define the error metric used to compare the various algorithms in Sec. II-D. K is the number of points within each subinterval where the potential value needs to be known. The coefficients c_k and a_{jk} are unique for each combination of r and J . We refer the reader to [8] for their derivation.

The integrator $\text{CF}_1^{[2]}$ is also sometimes referred to as the exponential midpoint rule. It was used in the context of NFT for the defocusing NSE ($\kappa = -1$) by Yamada and Sakuda [43] and later by Boffetta and Osborne [10]. For $\text{CF}_1^{[2]}$, Eq. 7 reduces to

$$\begin{aligned}\hat{\phi}_{n+1}(\lambda) &= G_n(\lambda) \phi_n(\lambda), \quad \text{where} \\ G_n(\lambda) &= \text{expm}(h C_n(\lambda)), \\ C_n(\lambda) &= \begin{bmatrix} -i\lambda & q_n \\ -\kappa q_n^* & i\lambda \end{bmatrix}.\end{aligned}\quad (10)$$

This is applied repeatedly as in Eq. 9 to obtain $\hat{\phi}(T_+, \lambda)$. In [14] we investigated the possibility of using $\text{CF}_2^{[4]}$ (first introduced in [34]) to obtain $\hat{\phi}(T_+, \lambda)$. We were able to show its advantage over $\text{CF}_1^{[2]}$ when considering the trade-off between an error and execution time. Here we investigate further in this direction and evaluate $\text{CF}_3^{[4]}$, $\text{CF}_3^{[5]}$ and $\text{CF}_4^{[6]}$, which are fourth-, fifth- and sixth-order methods respectively. The CFQM exponential integrators require multiple non-equispaced points within each subinterval. However, it is unrealistic to assume that signal samples at such non-equispaced points can be obtained in a practical setting. Hence in [14] we proposed the use of local cubic-spline based interpolation to obtain the non-equispaced points from the mid-points of each subinterval. We will refer to the samples at these midpoints as the given samples. Although the use of a local cubic-spline based interpolation was found to be sufficiently accurate for $\text{CF}_2^{[4]}$, it is insufficient for higher-order methods. Here, we propose to combine bandlimited interpolation with the time-shift property of Fourier transform, i.e.,

$$q(t - t_s) = \mathcal{F}^{-1}(e^{-i\xi t_s} \mathcal{F}(q(t))), \quad (11)$$

to obtain the irregularly spaced samples. This interpolation rule is accurate when $q(t)$ is sampled in accordance with the Nyquist criterion. As we are working with discrete signal samples, the interpolation can be implemented efficiently using fast Fourier transform (FFT).

D. Error Metric and Numerical Examples

In this section, we compare the performance of CFQM exponential integrators $\text{CF}_1^{[2]}$, $\text{CF}_2^{[4]}$, $\text{CF}_3^{[4]}$, $\text{CF}_3^{[5]}$ and $\text{CF}_4^{[6]}$, the two-step Implicit-Adams method (IA₂) introduced in [36] and the fourth-order Runge-Kutta method [13] (RK₄) for computation of the reflection coefficient. The fourth-order Runge-Kutta method ($r = 4$) was the first fourth-order method used for computation of reflection coefficient in [13], [45]. We include the third-order two-step Implicit-Adams method ($r = 3$) here as it was the first time a higher-order method was introduced in the context of fast nonlinear Fourier transform. The meaning of "fast" will be made precise in Sec. III.

We are interested in evaluating the trade-off between the increased accuracy and execution time due to use of higher-order methods. We assess the accuracy of different methods using the relative L^2 -error

$$E_\rho = \frac{\sum_{n=0}^{M-1} |\rho(\lambda_n) - \hat{\rho}(\lambda_n)|^2}{\sum_{n=0}^{M-1} |\rho(\lambda_n)|^2}, \quad (12)$$

where $\rho(\lambda)$ is the analytical reflection coefficient, $\hat{\rho}(\lambda)$ is the numerically computed reflection coefficient and λ_n are M equally-spaced points in $[-\lambda_{\max}, \lambda_{\max}]$. E_ρ is a global error and hence it is expected to be $\mathcal{O}(h^r)$ for an integrator of order r as explained in Sec. II-C. We fixed $M = 2^9$ to ensure acceptable execution times for the numerical tests.

1) *Example 1: Hyperbolic Secant*, $\kappa = 1$: As the first numerical example we chose the signal $q(t) = \tilde{q} e^{-2i\lambda_0 t} \text{sech}(t)$. The closed form of the reflection coefficient is given by applying the frequency-shift property [44, Sec. D] to the

analytical known reflection coefficient of the secant-hyperbolic signal [29],

$$\begin{aligned}\rho(\lambda) &= \frac{b(\lambda)}{a(\lambda)}, \\ b(\lambda) &= \frac{-\sin(\hat{q}\pi)}{\cosh(\pi(\lambda - \lambda_0))}, \\ a(\lambda) &= \frac{\Gamma^2(0.5 - i\lambda)}{\Gamma(0.5 - i(\lambda - \lambda_0) + \hat{q})\Gamma(0.5 - i(\lambda - \lambda_0) - \hat{q})},\end{aligned}\quad (13)$$

where $\Gamma(\cdot)$ is the gamma function. The discrete spectrum is

$$\lambda_k = \lambda_0 + i(\hat{q} + 0.5 - k), \quad k = 1, 2, \dots, M_D, \quad (14)$$

$$b_k = (-1)^k, \quad k = 1, 2, \dots, M_D, \quad (15)$$

$$M_D = \lfloor (\hat{q} + 0.5) \rfloor. \quad (16)$$

We set $\hat{q} = 5.4$, $\lambda_0 = 3$, $\lambda_{\max} = 10$, and chose $[T_-, T_+] = [-32, 32]$ to ensure negligible truncation error.

2) *Example 2: Rational Reflection Coefficient with one pole*, $\kappa = 1$: The signal is given by [28]

$$q(t) = \begin{cases} -2i\gamma \frac{\alpha}{|\alpha|} \operatorname{sech}\left(2\gamma t + \operatorname{arctanh}\left(\frac{\beta}{\gamma}\right)\right), & t \leq 0 \\ 0, & t > 0, \end{cases} \quad (17)$$

where α, β are scalar parameters and $\gamma = \sqrt{\alpha\alpha^* + \beta^2}$. We used $\alpha = 1$ and $\beta = -1$. The corresponding reflection coefficient is then known to be

$$\rho(\lambda) = \frac{\alpha}{\lambda - i\beta}. \quad (18)$$

We set $\lambda_{\max} = 60$ and chose $[T_-, T_+] = [-12, 0]$. As the signal in Eq. 17 has a discontinuity, it cannot be interpolated well using bandlimited interpolation. We hence assume only in this example that we can sample the signal at exactly the points that we require.

3) *Example 3: Hyperbolic Secant*, $\kappa = -1$: The signal is given by

$$q(t) = \frac{\mathcal{Q}}{L} \left(\operatorname{sech}\left(\frac{t}{L}\right) \right)^{1-2i\mathcal{F}}, \quad (19)$$

where \mathcal{F}, \mathcal{L} and \mathcal{Q} are scalar parameters. We used $\mathcal{F} = 1.5$, $\mathcal{L} = 0.04$ and $\mathcal{Q} = 5.5$. The corresponding reflection coefficient is known to be [25]

$$\rho(\lambda) = -2^{-2i\mathcal{F}} \mathcal{Q} \frac{\Gamma(d)\Gamma(f_-)\Gamma(f_+)}{\Gamma(d^*)\Gamma(g_-)\Gamma(g_+)}, \quad (20)$$

where $\Gamma(\cdot)$ is the gamma function, $d = 0.5 + i(\lambda\mathcal{L} - \mathcal{F})$, $f_{\pm} = 0.5 - i(\lambda\mathcal{L} \pm \sqrt{\mathcal{F}^2 + \mathcal{Q}^2})$, and $g_{\pm} = 1 - i(\mathcal{F} \pm \sqrt{\mathcal{F}^2 + \mathcal{Q}^2})$. We set $\lambda_{\max} = 250$ and chose $[T_-, T_+] = [-1.5, 1.5]$.

The numerical methods were implemented in MATLAB using the exact representation of a 2×2 matrix exponential in [6] for the CFQM exponential integrators. The execution times for each method were recorded using the MATLAB stopwatch function (tic-toc). The execution times are of course implementation-specific, but we tried to make the implementations as comparable as possible. Fig. 1 shows the error measure E_ρ , as defined in Eq. 12, for Example 1 for a range of relatively large sampling intervals h . These results suggest

that the higher-order methods can always be preferred over the lower-order methods. The error measure E_ρ for smaller sampling intervals h for Example 1, 2 and 3 are shown in Figs. 2, 3 and 4 respectively. To ensure that the discontinuity in Example 2 is faithfully captured, we use a slightly different time grid for the Runge-Kutta method and the Implicit-Adams method, compared to the description in Sec. II-A. For all three examples, the slopes of the error-lines are in agreement with the order r of each method except for IA_2 . For smooth signals IA_2 is seen to have an error of order four rather than the expected three. This observation is in agreement with [36, Fig. 2]. However, for the discontinuous signal of Example 2 we see third-order behavior as expected. We can also see that a higher r generally corresponds to better accuracy (lower E_ρ) for the same h . However, that is not necessarily obvious as seen in Fig. 2, where $\text{CF}_3^{[5]}$ is more accurate than $\text{CF}_4^{[6]}$ for larger h . The advantage of using three exponentials ($J = 3$) in $\text{CF}_4^{[3]}$ instead of two in $\text{CF}_4^{[2]}$ is also clear from the figures. The third-order Implicit-Adams method (IA_2 with $r = 3$) and fourth-order Runge-Kutta method (RK_4) may be more accurate than $\text{CF}_2^{[1]}$ depending on the signal and other parameters, but have lower accuracy compared to $\text{CF}_4^{[2]}$ and $\text{CF}_4^{[3]}$. The error E_ρ reaches a minimum around 10^{-12} and can start rising again as seen in Fig. 4 for $\text{CF}_6^{[4]}$. To understand this behavior, note that the error per layer in Eq. 7 is actually $\mathcal{O}(h^{r+1} + \varepsilon)$, where ε is a small constant due to finite precision effects that can normally be neglected. The total error is thus $\mathcal{O}(h^r + \varepsilon h^{-1})$. As h is becoming smaller and smaller, the second component also known as the arithmetic error, becomes dominant and eventually causes the total error to rise again [22].

For the CFQM exponential integrators, computation of the transfer-matrix $H(\lambda)$ in Eq. 9 for each λ requires JD multiplications of 2×2 matrices (Eq. 7) for $D(\propto 1/h)$ given samples. If the reflection coefficient is to be computed at M points then the overall computational complexity will be of the order $\mathcal{O}(DM)$, because $J \ll D$. In Fig. 5 we plot the execution times of all the methods for Example 1. These execution times are representative for all examples. We can see that the execution time scales linearly with D as expected since M is kept constant in the numerical examples. The execution time of the CFQM exponential integrators is also a linear function of J . The IA_2 , RK_4 and $\text{CF}_4^{[2]}$ methods have similar execution times. To evaluate the trade-off between the execution time and accuracy, we plot the execution time on the x-axis and the error on the y-axis in Fig. 6 for Example 1. To read such trade-off plots we look at the error achieved by each method for a given amount of time. For Example 1 it turns out that $\text{CF}_5^{[3]}$ provides the best trade-off, but we can conclude that extra computation cost of the higher-order methods is generally justified by increased accuracy.

If M is of the same order as D then the computational complexity of the NFT will be $\mathcal{O}(D^2)$. Although performing matrix multiplications of 2×2 matrices is fast, the total cost of the NFT is significantly higher when compared to its linear analogue, the FFT, which has a complexity of only $\mathcal{O}(D \log D)$. So the natural question to ask is; Can the complexity be reduced?

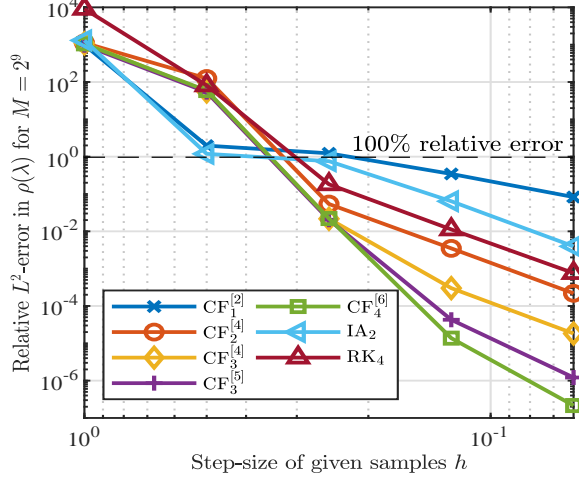


Fig. 1. Error using slow NFT algorithms for Example 1 with $\lambda_{\max} = 1$.

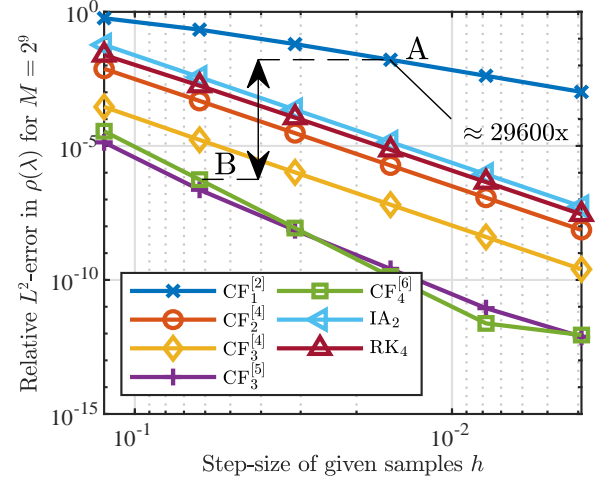


Fig. 2. Error using slow NFT algorithms for Example 1 with $\lambda_{\max} = 10$. A and B have identical computation times.

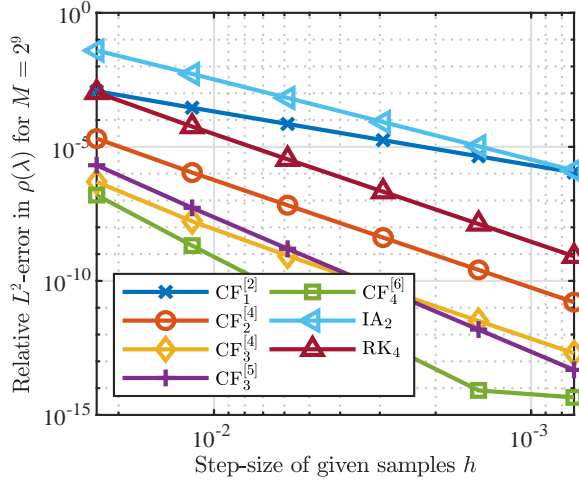


Fig. 3. Error using slow NFT algorithms for Example 2.

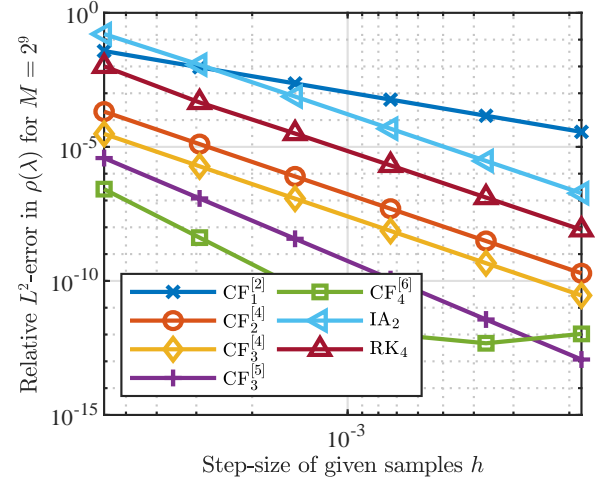


Fig. 4. Error using slow NFT algorithms for Example 3.

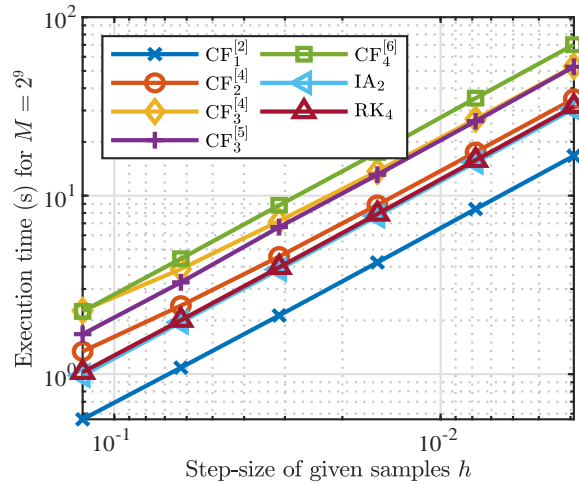


Fig. 5. Execution time using slow NFT algorithms for Example 1.

III. FAST NONLINEAR FOURIER TRANSFORM

The complexity of the new NFTs proposed in the previous section is quadratic in the number of given samples, $\mathcal{O}(D^2)$. In this section, we demonstrate how the complexity of some of them can be reduced to $\mathcal{O}(D \log^2 D)$ by integrating them into the framework in [41], [42].

A. Fast Scattering Framework

In the framework proposed in [41], each matrix $G_n(\lambda)$ is approximated by a rational function matrix $\hat{G}_n(z)$, where $z = z(\lambda)$ is a transformed coordinate. By substituting these approximations in Eq. 9, a rational function approximation $\hat{H}(z)$ of $H(\lambda)$ is obtained.

$$\hat{H}(z) = \prod_0^{D-1} \hat{G}_n(z) \quad (21)$$

We want to compute the coefficients of the numerator and denominator polynomials, respectively. A straightforward implementation of the matrix multiplication where each entry

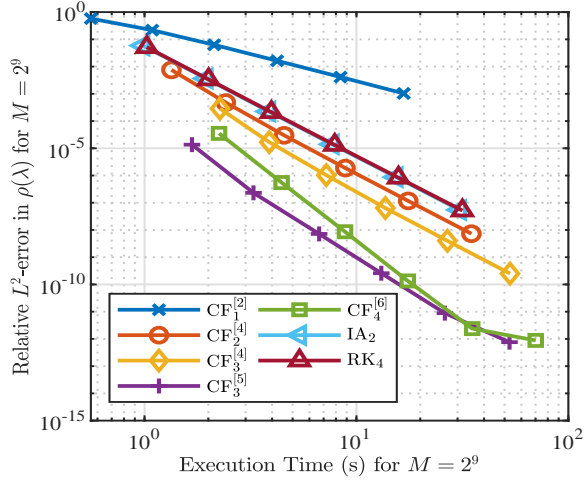


Fig. 6. Error vs. Execution time trade-off using slow NFT algorithms for Example 1.

is a polynomial has a complexity of $\mathcal{O}(D^2)$. Instead, by using a binary-tree structure and FFTs [41, Alg. 1], the computational complexity can be reduced to $\mathcal{O}(D \log^2 D)$. Hence it is referred to as fast scattering. The resulting rational function approximation $\hat{H}(z)$ is explicitly parametrized in z and hence Eq. 9 is reduced to polynomial evaluations for each z . To elaborate, we again restrict ourselves to $G_n(\lambda)$ of the form Eq. 7. Hence for $\text{CF}_1^{[2]}$, we need to approximate $G_n(\lambda) = \text{expm}(hC_n(\lambda))$. The matrix exponential can be approximated to various orders of accuracy using rationals [9] or using splitting-schemes such as the well-known Strang-splitting. Higher-order splitting-schemes were developed in [26] that map $\lambda \in \mathbb{R}$, the domain of the reflection coefficient, to $z = \exp(i\lambda h/m)$ on the unit circle, where m is a real rational. Such mappings have a certain advantage when it comes to polynomial evaluations which we cover in Sec. III-B. For a higher-order $\text{CF}_J^{[r]}$ integrator, each $G_n(\lambda)$ is a product of J matrix exponentials. For example let us look at $\text{CF}_2^{[4]}$. We can write

$$\begin{aligned} G_n(\lambda) &= \text{expm}(hC_n^2(\lambda)) \text{expm}(hC_n^1(\lambda)), \\ C_n^2(\lambda) &= a_2 C(T_- + (n+c_1)h, \lambda) + a_1 C(T_- + (n+c_2)h, \lambda), \\ C_n^1(\lambda) &= a_1 C(T_- + (n+c_1)h, \lambda) + a_2 C(T_- + (n+c_2)h, \lambda), \\ a_1 &= \frac{1}{4} + \frac{\sqrt{3}}{6}, \quad a_2 = \frac{1}{4} - \frac{\sqrt{3}}{6}, \\ c_1 &= \frac{1}{2} - \frac{\sqrt{3}}{6}, \quad c_2 = \frac{1}{2} + \frac{\sqrt{3}}{6}. \end{aligned} \quad (22)$$

Each of the two matrix exponentials can be approximated individually using a splitting-scheme from [26]. $\hat{H}(z)$ can then be obtained as in Eq. 21. However, there are a few caveats which prevent extension of this idea to higher-order methods. The splitting-schemes in [26] should not be applied to CFQM exponential integrators with complex coefficients a_{jk} . Complex coefficients mean that $\lambda \in \mathbb{R}$ is no longer mapped to z on the unit circle. Such a mapping is undesirable for polynomial evaluation as will be explained in Sec. III-B. In addition, we do not even obtain a polynomial structure if there

exists no z such that $\exp(i\lambda h \sum_{k=1}^K a_{j,k})$ is an integer power of this z for all j . Furthermore, if such a z exists but only for high co-prime integer powers, $\hat{G}_n(\lambda)$ will consist of sparse polynomials of high degree, which can significantly hamper the computational advantage of using the approximation. Due to these reasons we restrict ourselves to fast implementations of $\text{CF}_1^{[2]}$ and $\text{CF}_2^{[4]}$ which will be referred to as $\text{FCF}_1^{[2]}$ and $\text{FCF}_2^{[4]}$. The $\text{FCF}_1^{[2]}$ algorithm is already available as a part of the FNFT software library [40]. However, accuracy and execution times for it haven't been published formally anywhere in literature. The $\text{FCF}_2^{[4]}$ algorithm is completely new. For both $\text{FCF}_1^{[2]}$ and $\text{FCF}_2^{[4]}$ we use the fourth-order accurate splitting [26, Eq. 20].

B. Fast Evaluation

Once we obtain the rational function approximation $\hat{H}(z)$ of $H(\lambda)$ in terms of numerator and denominator coefficients, we only have to evaluate the numerator and denominator functions for each value of $z = z(\lambda)$ in order to compute the reflection coefficient. The degree of the polynomials to be evaluated will be at least D which can be in the range of 10^3 - 10^4 . It is known that evaluation of such high-degree polynomials for large values of z can be numerically problematic [42, Sec. IV.E]. However, by choosing the mapping $z = \exp(i\lambda h/m)$, which maps the real line to the unit circle, the polynomials need to be evaluated on the unit circle where evaluation of even high-degree polynomials is numerically easier. The higher-order splitting schemes in [26] were developed with such a mapping in mind allowing for approximations of the matrix exponentials as rational functions in z . Evaluating any polynomial of degree D using Horner's method has a complexity of $\mathcal{O}(D)$. Hence for M values of z , the total cost of fast scattering followed by polynomial evaluation will be $\mathcal{O}(D \log^2 D + MD)$. Mapping $\lambda \in \mathbb{R}$ to z on the unit circle has an additional computational advantage. Let $p(z) = p_N z^N + p_{N-1} z^{N-1} + \dots + p_0$ be a polynomial in z of degree N . Evaluation of $p(z)$ at a point z_k can be written as

$$p(z_k) = \sum_{n=0}^N p_n z_k^n = z_k^N \sum_{n=0}^N p_{N-n} z_k^{-n}. \quad (23)$$

For M points z_k , $k = 1, \dots, M$ on the unit circle, this is equivalent to taking the Chirp Z-transform (CZT) of the polynomial coefficients along an appropriately defined contour. The CZT can be computed efficiently using the algorithm in [27] which utilizes FFT's. We can also see Eq. 23 as a non-equispaced discrete Fourier transform (NDFT) of the polynomial coefficients which allows us to utilize efficient NFFT algorithms in [20] for evaluating the polynomial. If the number of evaluation points M is in the same order of magnitude as D , the complexity of evaluation becomes $\mathcal{O}(D \log D)$ and hence the overall complexity of the fast nonlinear Fourier transform (FNFT) is $\mathcal{O}(D \log^2 D)$.

C. Numerical Examples

We implemented $\text{FCF}_1^{[2]}$ and $\text{FCF}_2^{[4]}$ using the fourth-order accurate splitting scheme [26, Eq. 20] and the fast polynomial

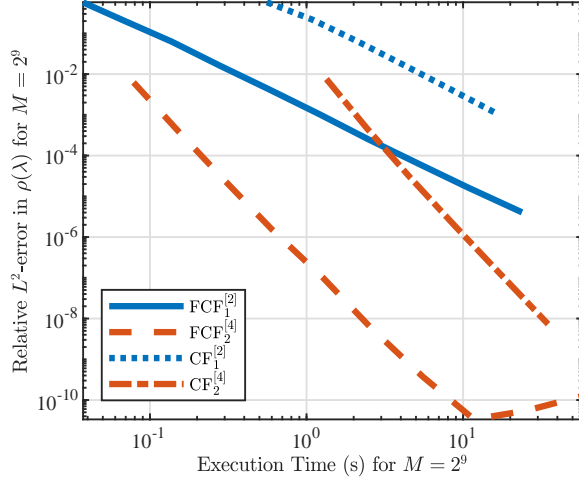


Fig. 7. Error vs. Execution time trade-off using CF and FCF algorithms for Example 1.

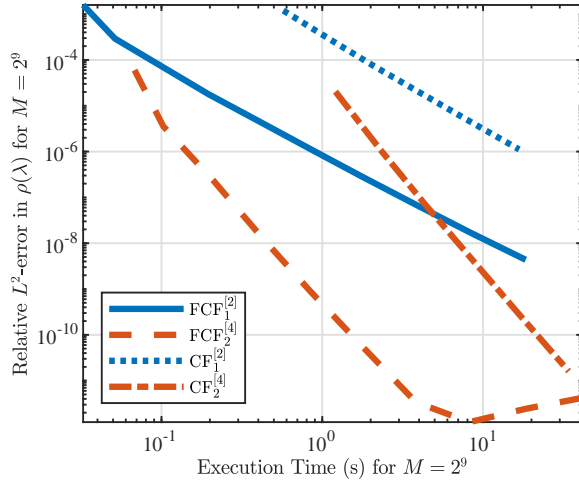


Fig. 8. Error vs. Execution time trade-off using CF and FCF algorithms for Example 2.

multiplication algorithm [41, Alg. 1]. We used the NDFT routine from [20] for evaluating the polynomials. Now we compare the implementations of $CF_1^{[2]}$ and $CF_2^{[4]}$ presented in Sec. II-D and their fast versions $FCF_1^{[2]}$ and $FCF_2^{[4]}$. We plot the error versus the execution time for Example 1 in Fig. 7, for Example 2 in Fig. 8 and for Example 3 in Fig. 9. In the three figures we can see that the fast FCF algorithms achieve similar errors as their slow CF counterparts in a significantly shorter time. From the other viewpoint, for the same execution time, the FCF algorithms achieve significantly lower errors compared to CF algorithms. The trade-off shifts further towards FCF algorithms as the number of evaluation points M increases. $FCF_2^{[4]}$ outperforms $FCF_1^{[2]}$ in the trade-off for both the examples which again highlights the advantage of using higher-order CFQM exponential integrators. $FCF_2^{[4]}$ reaches a minimum error around 10^{-11} and then starts rising. This is again attributed to the arithmetic error becoming the dominant source of error. We remark that in numerical tests the CZT was found to perform equally well as the NDFT

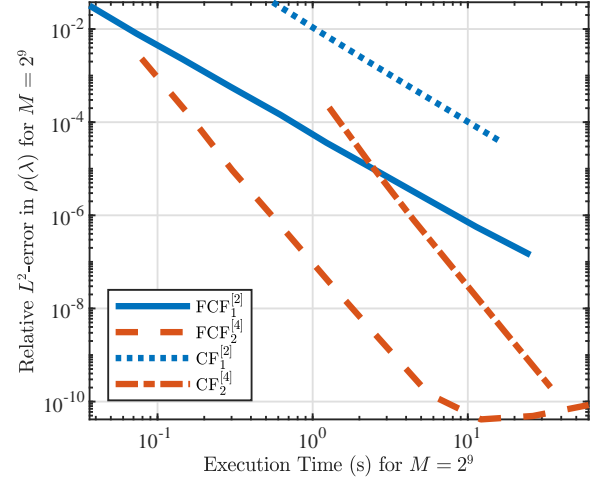


Fig. 9. Error vs. Execution time trade-off using CF and FCF algorithms for Example 3.

before the error minimum but the error rise thereafter was significantly steeper.

Since the NFT is a nonlinear transform, it changes its form under scaling, and computing it typically becomes increasingly difficult when being scaled up [37]. Hence it is of interest to study scaling of error with increase in signal energy. To test the scaling we use Example 1 and sweep the signal amplitude \hat{q} from 0.4 to 10.4 in steps of 1.0 while keeping all other parameters the same as before. As the time-window remains the same, scaling the signal amplitude leads to directly proportional scaling of the signal energy. We compute the error E_ρ for decreasing h for each value of \hat{q} for the CF and FCF algorithms. We plot E_ρ versus the sampling interval h on a log-scale for CF algorithms in Fig. 10 and for FCF algorithms in Fig. 11. Instead of plotting individual lines for each value of \hat{q} , we represent the amplitude using different shades of gray. As shown in the colourbar, lighter shades represents lower \hat{q} and darker shades represent higher \hat{q} . The stripes with a higher slope are the higher-order methods. The piecewise constant signal approximation becomes less accurate with increasing signal amplitude, which directly translates to a higher error E_ρ for larger values of \hat{q} . All the four algorithms i.e., $CF_1^{[2]}$, $CF_2^{[4]}$, $FCF_1^{[2]}$ and $FCF_2^{[4]}$ show similar trends for the scaling of error with signal energy. The $CF_1^{[2]}$ algorithm was compared with other methods in [37] (where it is referred to as BO), and they conclude that $CF_1^{[2]}$ scales the best with increasing signal amplitude. Hence the results shown in Fig. 10 are very motivating as $CF_2^{[4]}$ is seen to scale almost as well as $CF_1^{[2]}$. The error of approximations used in the FCF algorithms also depends on \hat{q} . However, comparing Fig. 10 and Fig. 11 we can see that the contribution of the approximation error is negligible. These results combined with the results in the trade-off plots (Figs. 7, 8 and 9) make a strong case for the $FCF_2^{[4]}$ algorithm.

As an efficient FNFT algorithm can be combined with the recently proposed b -modulation [19], [21], [39] scheme to develop a complete NFT based fiber-optic communication sys-

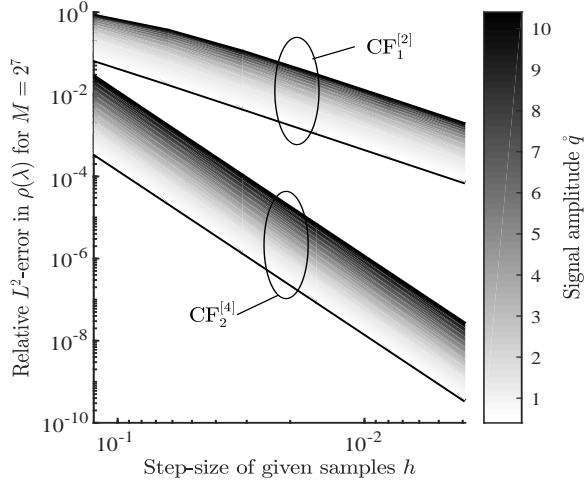


Fig. 10. Variation of error of CF algorithms with amplitude for Example 1. The fourth-order $CF_2^{[4]}$ algorithm is seen to have gradual increase in error with increase in amplitude similar to the second-order $CF_1^{[2]}$ algorithm.

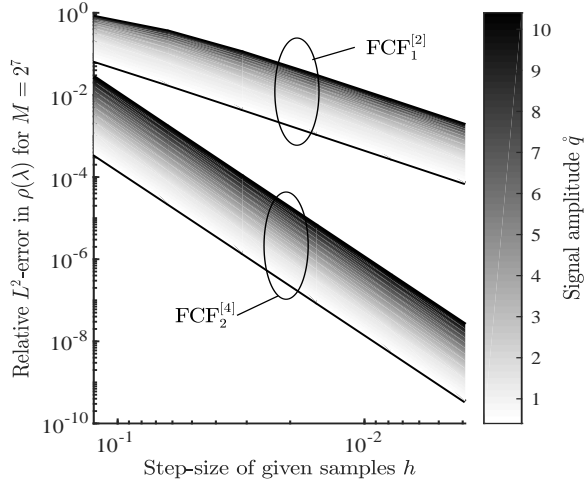


Fig. 11. Variation of error of FCF algorithms with amplitude for Example 1. Approximating the matrix exponentials with splitting schemes does not significantly affect the scaling of error with increasing amplitude.

tem, accurate and fast computation of the scattering coefficient $b(\lambda)$ is of interest. Hence to test the performance of both the FCF algorithms in computation of b -coefficient, we define

$$E_b = \frac{\sum_{n=0}^{M-1} |b(\lambda_n) - \hat{b}(\lambda_n)|^2}{\sum_{n=0}^{M-1} |b(\lambda_n)|^2}, \quad (24)$$

where $b(\lambda)$ is the analytically known and $\hat{b}(\lambda)$ is the numerically computed scattering coefficient. For the numerical test we again use the signal from Example 1 as $b(\lambda)$ is known. We plot the error E_b for both the FCF methods for decreasing sampling interval h in Fig. 12. $FCF_2^{[4]}$ clearly outperforms $FCF_1^{[2]}$ even after considering the additional computational cost.

From the results of the numerical tests presented in this section it is clear that approximating $H(\lambda)$ in Eq. 9 using rational functions provides a significant computational advantage. However, as mentioned earlier we have had to restrict

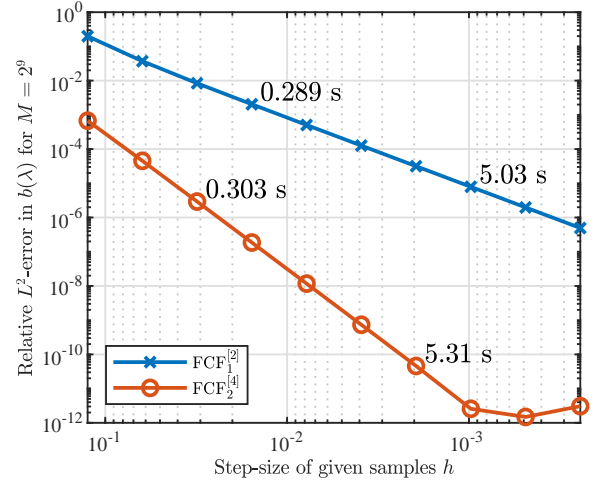


Fig. 12. Error in b -coefficient using FCF algorithms for Example 1. The execution times for some of the points are shown to give an indication of the computational complexity.

ourselves to fourth-order method $FCF_2^{[4]}$. To further improve the accuracy and order of convergence while restricting ourselves to a fourth-order method, we explore the possibility of using series acceleration techniques in the next section.

IV. SERIES ACCELERATION

Series acceleration methods are techniques for improving the rate of convergence of a series. In particular, they were used to improve an inverse NFT algorithm for the defocusing case in [15]. Series acceleration was also used to improve the accuracy of the split-step Fourier algorithm [32] commonly used to solve the NSE directly. Here we study the applicability of a specific series acceleration technique known as the Richardson extrapolation [30] to the FCF algorithms.

A. Richardson Extrapolation

Given an r^{th} -order numerical approximation method $\hat{\rho}(\lambda, h)$ for $\rho(\lambda)$ that depends on the step-size h , we can write

$$\rho(\lambda) = \hat{\rho}(\lambda, h) + \mathcal{O}(h^r). \quad (25)$$

We assume that $\hat{\rho}(\lambda, h)$ has series expansion in h ,

$$\hat{\rho}(\lambda, h) = \rho(\lambda) + \rho_r(\lambda)h^r + \rho_{r+1}(\lambda)h^{r+1} + \dots \quad (26)$$

In Richardson extrapolation [30], we combine two numerical approximations $\hat{\rho}(\lambda, h)$ and $\hat{\rho}(\lambda, 2h)$ as follows,

$$\hat{\rho}^{[\text{RE}]}(\lambda, h) = \frac{2^r \hat{\rho}(\lambda, h) - \hat{\rho}(\lambda, 2h)}{2^r - 1}. \quad (27)$$

Using the series expansion, we find that the order of the new approximation $\hat{\rho}^{[\text{RE}]}(\lambda, h)$ is at least $r + 1$:

$$\begin{aligned} \hat{\rho}^{[\text{RE}]}(\lambda, h) &= \frac{2^r(\rho(\lambda) + \rho_r(\lambda)h^r + \rho_{r+1}(\lambda)h^{r+1} + \dots)}{2^r - 1} \\ &\quad - \frac{\rho(\lambda) + \rho_r(\lambda)(2h)^r + \rho_{r+1}(\lambda)(2h)^{r+1} + \dots}{2^r - 1} \\ &= \rho(\lambda) - \frac{2^r}{2^r - 1} \rho_{r+1}(\lambda)h^{r+1} + \mathcal{O}(h^{r+2}). \end{aligned} \quad (28)$$

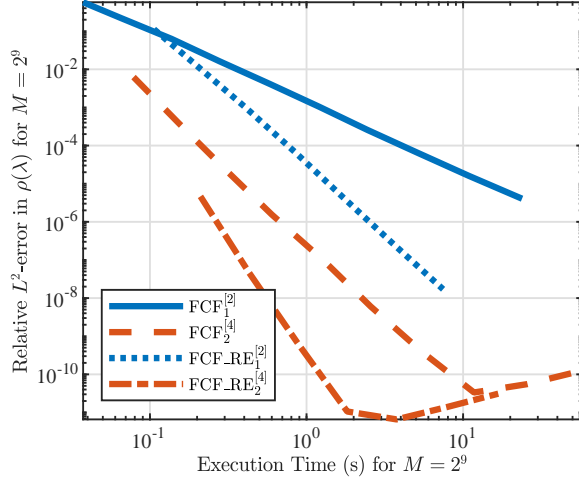


Fig. 13. Error vs. Execution time trade-off of FCF and FCF_RE algorithms for Example 1.

We apply this idea to $\text{FCF}_1^{[2]}$ and $\text{FCF}_2^{[4]}$ to obtain $\text{FCF_RE}_1^{[2]}$ and $\text{FCF_RE}_2^{[4]}$ algorithms. We remark that series acceleration can also be applied to the slow algorithms in Sec. II-C.

B. Numerical examples

We test $\text{FCF_RE}_1^{[2]}$ and $\text{FCF_RE}_2^{[4]}$ against $\text{FCF}_1^{[2]}$ and $\text{FCF}_2^{[4]}$ for all three examples. Since Richardson extrapolation requires us to compute two approximations, which increases the computational complexity, we again evaluate the complexity-accuracy trade-off. We plot the error versus execution time curves for the three examples in the Figs. 13 to 15. In all figures we can see that the FCF_RE algorithms achieve slopes of $r+2$ rather than the expected slope of $r+1$. This is an example of superconvergence [33]. Specifically, the error of $\text{FCF_RE}_1^{[2]}$ decreases with slope four and that of $\text{FCF_RE}_2^{[4]}$ decreases with slope six. As seen before in Sec. II-D, the arithmetic error starts to dominate after a certain point and causes the error to rise. Although the executions times of FCF_RE algorithms are higher, the error achieved is almost an order of magnitude lower even for large h . From the other viewpoint, for the same execution time, the FCF_RE algorithms achieve significantly lower errors compared to FCF algorithms. $\text{FCF_RE}_2^{[4]}$ outperforms $\text{FCF_RE}_1^{[2]}$ in the trade-off for all the three examples again highlighting the advantage of using higher-order CFQM exponential integrators. These results suggest that Richardson extrapolation should be applied to improve the considered FNFT algorithms. The $\text{FCF_RE}_2^{[4]}$ algorithm provides the best trade-off among all the algorithms presented in this paper.

V. COMPUTING EIGENVALUES

Recall that for the case of focusing NSE ($\kappa = 1$), the nonlinear Fourier spectrum has two parts: a continuous and a discrete part. In this section, we are concerned with the numerical computation of the discrete part. We first mention some of the existing approaches and then show how one of them can be extended to work with the new fast higher-order

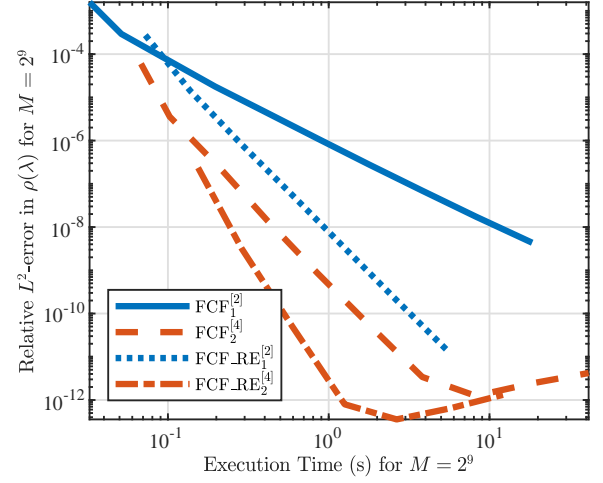


Fig. 14. Error vs. Execution time trade-off of FCF and FCF_RE algorithms for Example 2.

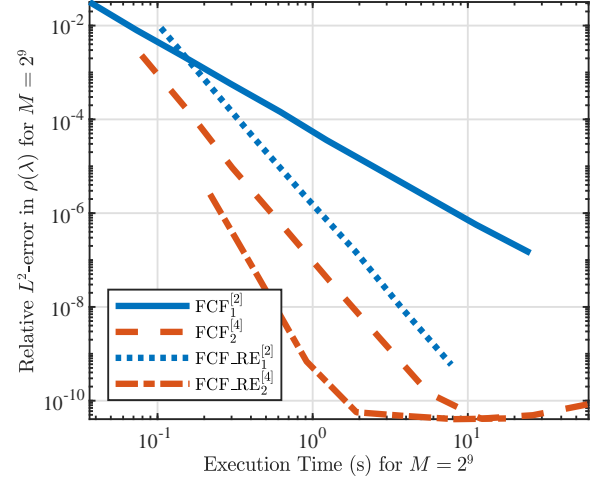


Fig. 15. Error vs. Execution time trade-off of FCF and FCF_RE algorithms for Example 3.

NFT algorithms. We will also show that Richardson extrapolation can be applied to improve the accuracy at virtually no extra computational cost.

A. Existing approaches

Finding the eigenvalues consists of finding the complex upper half-plane roots of the function $a(\lambda)$. Most of the existing approaches can be classified into four main categories.

- 1) *Search methods*: Newton's method.
- 2) *Eigenmethods*: Spectral methods based on the solution of a suitably designed eigenproblem [44].
- 3) *Gridding methods*: They find λ_k using iterative methods or optimized grid search [13], [44]. Recently a method based on contour integrals was proposed [38].
- 4) *Hybrid methods*: Any combination of the above. Eigenmethods with rougher sampling can e.g. be used to find initial guesses for a search method [4].

Our proposed method will be a hybrid of a eigenmethod and a search method in the spirit of [4], where an eigenproblem is solved to obtain initial guesses for Newton's method.

B. Proposed method

Remember that the discrete spectrum consists of eigenvalues, which are the zeros of $a(\lambda)$ in the complex upper half-plane (\mathbb{H}), and their associated norming constants. We start with discussing an approximation of $a(\lambda)$ that will be useful for locating the eigenvalues. From Eqs. 3, 4 and 5 we can write

$$a(\lambda) = \lim_{t \rightarrow \infty} \phi_1(t, \lambda) e^{i\lambda t}. \quad (29)$$

Over the finite interval $[T_-, T_+]$ using Eq. 9 we can see that

$$a(\lambda) \approx H_{1,1}(\lambda) e^{i\lambda T_-} e^{i\lambda T_+}. \quad (30)$$

Hence we hope that the zeros of $H_{1,1}(\lambda)$ are approximations of the zeros of $a(\lambda)$ if the signal truncation and discretization errors are small enough. In Sec. III-A we explained how $H(\lambda)$ can be approximated by a rational function in a transformed co-ordinate z . Hence we can further write

$$a(\lambda) \approx \frac{\hat{a}_{\text{num}}(z)}{\hat{a}_{\text{den}}(z)} e^{i\lambda T_-} e^{i\lambda T_+}, \quad (31)$$

where $\hat{a}_{\text{num}}(z)$ and $\hat{a}_{\text{den}}(z)$ are polynomials in $z(\lambda)$. Let $\hat{a}_{\text{num}}(z) = \hat{a}_N z^N + \hat{a}_{N-1} z^{N-1} + \dots + \hat{a}_0$. Thus $\hat{a}_{\text{num}}(z)$ will have N zeros. These zeros or roots of $\hat{a}_{\text{num}}(z)$ can be found using various methods [23]. Of these N zeros, there should be K (typically, $K \ll N$) values that are approximations of zeros of $a(\lambda)$ in \mathbb{H} .

Example: We would like to add clarity through a visual representation of the roots. We choose the signal from Example 1 with $D = 2^9$. We plot all the zeros of $\hat{a}_{\text{num}}(z)$ of $\text{FCF}_1^{[2]}$ with ‘x’ in Fig. 16. Here $z = e^{i\lambda h}$. We can then map these zeros back to obtain values of λ . These are plotted with ‘x’ in Fig. 17. From the definition of discrete spectrum, we can filter out all the values that are not in \mathbb{H} . We then filter further and keep only values of λ such that $|\text{Re}(\lambda)| < 0.9\pi/h$ which is close to a limit imposed by the chosen mapping from $z \rightarrow \lambda$. The filtered roots are plotted in Figs. 17 and 16 with ‘o’. For the chosen value of $\hat{q} = 5.4$ the set of eigenvalues is $\Lambda = \{3 + 4.9i, 3 + 3.9i, 3 + 2.9i, 3 + 1.9i, 3 + 0.9i\}$. From Fig. 17 we see that the values marked with ‘o’ are indeed approximations of the values in set Λ . However, there is no guarantee that we will always be able to locate approximations for all values in Λ as that depends on several factors, some of which are the signal magnitude q_o , signal interval $[T_-, T_+]$, step-size h and values of the eigenvalues themselves.

For the example chosen in the visual demonstration, the number of zeros is $N = 1024$ and the number of eigenvalues is $K = 5$. For the chosen mapping from $\lambda \rightarrow z$, the K values of interest will always lie inside the unit circle in Fig. 16 and most other spurious zeros of $\hat{a}_{\text{num}}(z)$ will lie on the unit circle. Even with the best eigenmethods available for polynomial root-finding, which have a complexity of $\mathcal{O}(N^2)$ [5], execution time grows very steeply, making this approach infeasible for large N . To reduce the complexity, it was suggested in [4] to sub-sample the given signal to reduce the dimensionality of the root-finding problem. The algorithm is summarized below.

Input: Samples q_0, \dots, q_{D-1} , D_{sub} , $[T_-, T_+]$

Output: Estimated eigenvalues $\hat{\lambda}_k$

- 1: Subsample the given samples $\rightarrow q_n^{\text{sub}} := q_{n \lfloor D/D_{\text{sub}} \rfloor}$. Build a polynomial approximation $\hat{a}_{\text{num}}(z)$ using the D_{sub} subsampled samples. Apply a fast eigenmethod to find the roots of $\hat{a}_{\text{num}}(z)$. Filter the roots.
- 2: Refine the roots via Newton’s method using all samples. Filter the refined roots.
- 3: Apply Richardson extrapolation to the unrefined and refined roots.

We now discuss the three stages of the algorithm in detail.

1) Root finding from subsampled signal

The given signal q_n is subsampled to give q_n^{sub} with D_{sub} samples. The corresponding step-size is h_{sub} . There are no results for the minimum number of samples that guarantee that all eigenvalues will be found. One choice can be based on limiting the overall computational complexity to $\mathcal{O}(D \log^2 D)$, which is the complexity for the reflection coefficient. For a root-finding algorithm with $\mathcal{O}(D^2)$ complexity, we choose to use $D_{\text{sub}} = \text{round}(\sqrt{D \log^2 D})$ samples. The polynomial $\hat{a}_{\text{num}}(z)$ is then built from these D_{sub} samples. For $\text{FCF}_2^{[4]}$, the non-equispaced samples should be obtained from the original D samples and not the D_{sub} samples. An eigenmethod is then used to find all zeros of $\hat{a}_{\text{num}}(z)$. We used the algorithm in [5]. The values of z are mapped backed to λ and filtered to remove implausible values.

2) Root refinement using Newton method

The Newton method based on the slow CF methods is used for root refinement. The derivative $\partial a(\lambda)/\partial \lambda$ is calculated numerically along with $a(\lambda)$ as in [10] using all the given samples q_n . The values of λ that remain after filtering in the previous step are used as the initial guesses for the Newton method. We chose to stop the iterations if the change in value goes below 10^{-15} or if a maximum of 15 iterations is reached. The resulting roots are filtered again.

3) Richardson extrapolation

We pair the roots resulting from the Newton step, $\hat{\lambda}_k^{\text{Newton}}$, with the corresponding initial guesses $\hat{\lambda}_k^{\text{init}}$. Then, we apply Richardson extrapolation:

$$\hat{\lambda}_k = \frac{\left(\frac{h_{\text{sub}}}{h}\right)^r \hat{\lambda}_k^{\text{Newton}} - \hat{\lambda}_k^{\text{init}}}{\left(\frac{h_{\text{sub}}}{h}\right)^r - 1}. \quad (32)$$

$\hat{\lambda}_k$ is then an improved approximation and constitutes the discrete part of the FCF-RE algorithm. It may so happen that more than one $\hat{\lambda}_k^{\text{init}}$ converge to the same $\hat{\lambda}_k^{\text{Newton}}$. In such cases the value $\hat{\lambda}_k^{\text{init}}$ closest to $\hat{\lambda}_k^{\text{Newton}}$ should be used for Richardson extrapolation. The other values $\hat{\lambda}_k^{\text{init}}$ that also converged to the same $\hat{\lambda}_k^{\text{Newton}}$ should be treated as spurious values and discarded.

The numerical algorithms may not find particular eigenvalues or find spurious ones. Let $\hat{\Lambda}$ be the set of approximations found

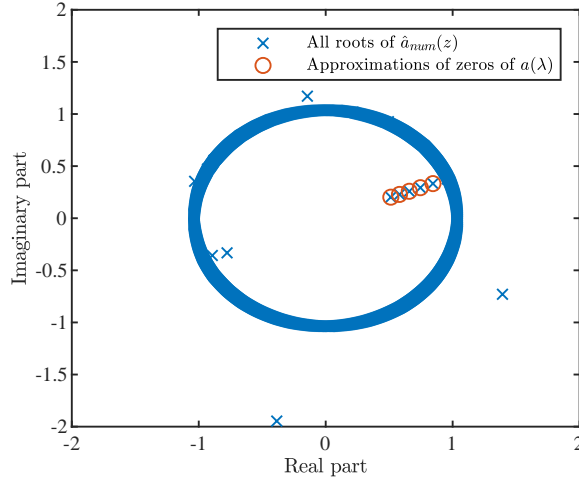


Fig. 16. Zeros of $\hat{a}_{\text{num}}(z)$ for Example 1 with $D = 2^9$.

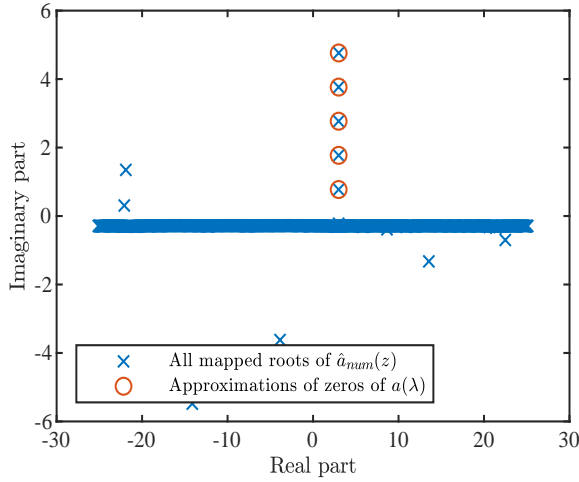


Fig. 17. Mapped zeros of $\hat{a}_{\text{num}}(z)$ for Example 1 with $D = 2^9$

by an algorithm. To penalize both missed values and incorrect spurious values at the same time, we define the error

$$E\Lambda = \max \left\{ \max_{\lambda_i \in \Lambda} \min_{\hat{\lambda}_j \in \hat{\Lambda}} |\lambda_i - \hat{\lambda}_j|, \max_{\hat{\lambda}_j \in \hat{\Lambda}} \min_{\lambda_i \in \Lambda} |\lambda_i - \hat{\lambda}_j| \right\}. \quad (33)$$

Note that the first term in the outer maximum grows large if an algorithm fails to approximate a part of the set Λ while the second term becomes large if an algorithm finds spurious values that have no correspondence with values in Λ . $E\Lambda$ is expected to be of order r for an algorithm of order r .

C. Numerical Example

In this section, we compare different variants of our proposed algorithm using Example 1. We compute the error $E\Lambda$ for the following three types of algorithms:

- 1) Discrete part of FCF algorithms. An eigenmethod is applied to the approximation $\hat{a}_{\text{num}}(z)$ built using all samples. No sub-sampling is used.

- 2) Discrete part of FCF algorithms with sub-sampling. Only steps 1 and 2 of the algorithm mentioned above.
- 3) Discrete part of FCF_RE algorithms. All the three steps mentioned above.

To demonstrate the effect of sub-sampling, we show in Fig. 18 the errors for the second- and fourth-order algorithms of types 1 and 2. For $h > 0.3$ the errors are high either due to failure to find approximations close to the actual eigenvalues or spurious values. For $h \leq 0.3$, $\text{FCF}_2^{[4]}$ of type 1 and $\text{FCF}_1^{[2]}$ of type 2 find exactly five values that are close approximations of the values in Λ . However $\text{FCF}_1^{[2]}$ of type 1 and $\text{FCF}_2^{[4]}$ of type 2 find good approximations only for $h \leq 0.06$. The error of $\text{FCF}_1^{[2]}$ algorithms decreases with slope two and that of $\text{FCF}_2^{[4]}$ algorithms decreases with slope four as expected from the order of the underlying numerical schemes.

In Fig. 19 we show the errors for the second- and fourth-order algorithms of type 2 and 3 to indicate the advantage of the extrapolation step. The extrapolation step improves the approximation significantly for $\text{FCF_RE}_1^{[2]}$ while adding negligible computation cost to the algorithm. However, there is only minor improvement in case of $\text{FCF_RE}_2^{[4]}$ over $\text{FCF}_2^{[4]}$.

In Fig. 20 we plot the execution times for the FCF algorithms of types 1 and 2. The execution times of algorithms of type 3 are almost the same as those of type 2. For type 1 algorithms, these times include the time required to build $\hat{a}_{\text{num}}(z)$ and the time taken by the root-finder. For algorithms of type 2, the additional time required for root-refinement by Newton's method is also included. Even with sub-sampling, we see that the execution times are an order of magnitude higher than the execution times for the continuous part. The FCF_RE algorithms seem to provide the best trade-off between accuracy and computation cost similar to the case of continuous part. The overall computational complexity may be decreased by using alternative methods to find the initial guesses.

VI. CONCLUSION

In this paper, we proposed new higher-order nonlinear Fourier transform algorithms based on a special class of exponential integrators. We also showed how some of these algorithms can be made fast using special higher-order exponential splittings. The accuracy of these fast algorithms was improved even further using Richardson extrapolation. Numerical demonstrations showed that the proposed algorithms are highly accurate and provide much better complexity-accuracy trade-offs than existing algorithms. In the future we plan to integrate the algorithms from this paper into the open source software library FNFT [40].

REFERENCES

- [1] M. J. Ablowitz, D. J. Kaup, A. C. Newell, and S. Harvey, "The Inverse Scattering Transform-Fourier Analysis for Nonlinear Problems," *Studies in Applied Mathematics*, vol. 53, no. 4, pp. 249–315, 1974.
- [2] G. P. Agrawal, *Fiber-Optic Communication Systems*, 4th ed. Hoboken, N.J., USA: Wiley, 2013.
- [3] E. Agrell *et al.*, "Roadmap of Optical Communications," *Journal of Optics*, vol. 18, no. 6, p. 063002, 2016.

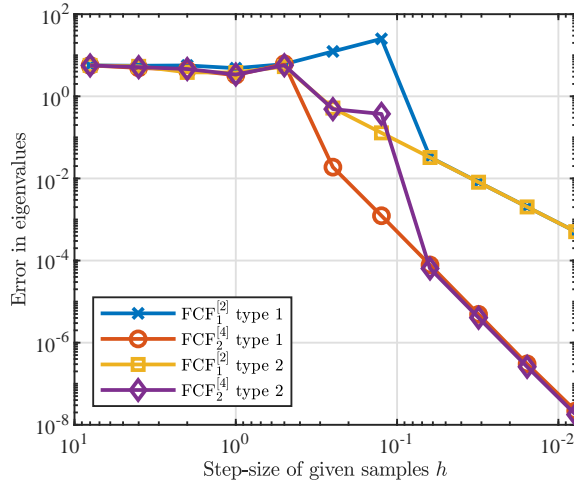


Fig. 18. Error in approximation of the eigenvalues by the fast second- and fourth-order algorithms of type 1 (no sub-sampling) and type 2 (sub-sample and refine, no Richardson extrapolation).

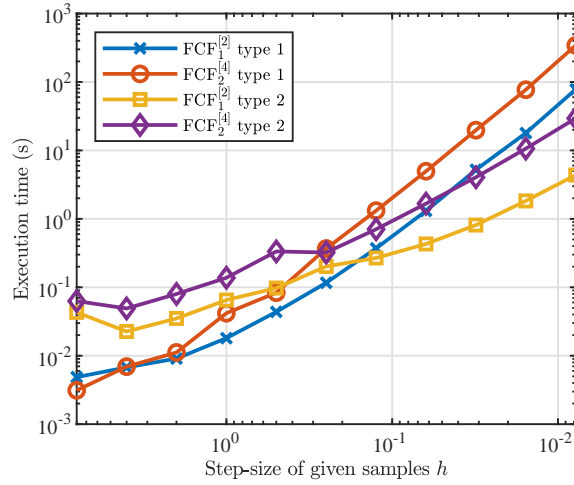


Fig. 20. Execution time of $FCF_2^{[4]}$ and $FCF_1^{[2]}$ algorithms for computing eigenvalues of Example 1.

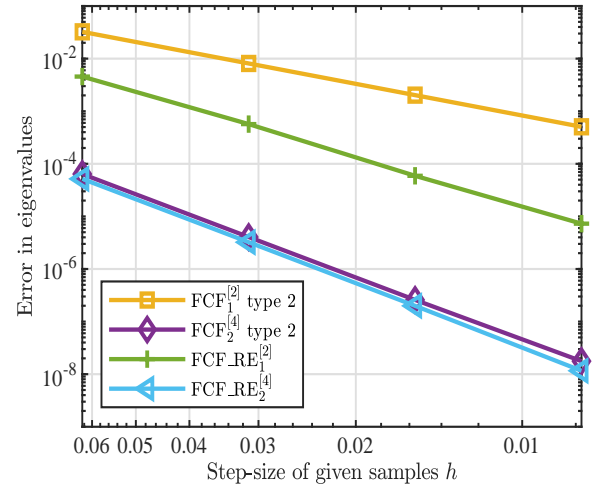


Fig. 19. Error in approximation of a eigenvalues computed using FCF and FCF_RE algorithms.

- [4] V. Aref, S. T. Le, and H. Buelow, "Modulation Over Nonlinear Fourier Spectrum: Continuous and Discrete Spectrum," *Journal of Lightwave Technology*, vol. 36, no. 6, pp. 1289–1295, March 2018.
- [5] J. Aurentz, T. Mach, R. Vandebril, and D. Watkins, "Fast and backward stable computation of roots of polynomials," *SIAM Journal on Matrix Analysis and Applications*, vol. 36, no. 3, pp. 942–973, 2015. [Online]. Available: <https://doi.org/10.1137/140983434>
- [6] D. S. Bernstein and W. So, "Some Explicit Formulas for the Matrix Exponential," *IEEE Transactions on Automatic Control*, vol. 38, no. 8, pp. 1228–1232, Aug 1993.
- [7] S. Blanes, F. Casas, J. Oteo, and J. Ros, "The Magnus Expansion and Some of its Applications," *Physics Reports*, vol. 470, no. 5, pp. 151 – 238, 2009.
- [8] S. Blanes, F. Casas, and M. Thalhammer, "High-order Commutator-free Quasi-Magnus Exponential Integrators for Non-autonomous Linear Evolution Equations," *Computer Physics Communications*, vol. 220, pp. 243 – 262, 2017.
- [9] J. L. Blue and H. K. Gummel, "Rational Approximations to Matrix Exponential for Systems of Stiff Differential Equations," *Journal of Computational Physics*, vol. 5, no. 1, pp. 70 – 83, 1970.
- [10] G. Boffetta and A. R. Osborne, "Computation of the Direct Scattering Transform for the Nonlinear Schrödinger Equation," *Journal of Computational Physics*, vol. 102, no. 2, pp. 252–264, 1992.
- [11] A. Bruckstein and T. Kailath, "An Inverse Scattering Framework for Several Problems in Signal Processing," *IEEE ASSP Magazine*, vol. 4, no. 1, pp. 6–20, Jan 1987.
- [12] M. Brühl, "Direct and Inverse Nonlinear Fourier Transform based on the Korteweg-deVries Equation (KdV-NLFT) - a Spectral Analysis of Nonlinear Surface Waves in Shallow Water," Ph.D. dissertation, Feb 2014.
- [13] S. Burtsev, R. Camassa, and I. Timofeyev, "Numerical Algorithms for the Direct Spectral Transform with Applications to Nonlinear Schrödinger Type Systems," *Journal of Computational Physics*, vol. 147, no. 1, pp. 166–186, 1998.
- [14] S. Chimmalgi, P. J. Prins, and S. Wahls, "Nonlinear Fourier Transform Algorithm Using a Higher Order Exponential Integrator," in *Advanced Photonics 2018*. Optical Society of America, 2018, p. SpM4G.5.
- [15] Y. Choi, J. Chun, T. Kim, and J. Bae, "The Schur Algorithm Applied to the One-Dimensional Continuous Inverse Scattering Problem," *IEEE Transactions on Signal Processing*, vol. 61, no. 13, pp. 3311–3320, 2013.
- [16] S. Civelli, S. K. Turitsyn, M. Secondini, and J. E. Prilepsky, "Polarization-multiplexed Nonlinear Inverse Synthesis with Standard and Reduced-complexity NFT Processing," *Optics Express*, vol. 26, no. 13, pp. 17 360–17 377, 2018.
- [17] C. L. Epstein, "How well does the finite Fourier transform approximate the Fourier transform?" *Communications on Pure and Applied Mathematics*, vol. 58, no. 10, pp. 1421–1435, 2005.
- [18] L. D. Faddeev and L. Takhtajan, *Hamiltonian Methods in the Theory of Solitons*. Springer-Verlag Berlin Heidelberg, 2007.
- [19] T. Gui, G. Zhou, C. Lu, A. P. T. Lau, and S. Wahls, "Nonlinear Frequency Division Multiplexing with b-Modulation: Shifting the Energy Barrier," *Opt. Express*, vol. 26, no. 21, pp. 27 978–27 990, Oct 2018.
- [20] J. Keiner, S. Kunis, and D. Potts, "Using NFFT 3- A Software Library for Various Nonequispaced Fast Fourier Transforms," *ACM Transactions on Mathematical Software*, vol. 36, no. 4, pp. 19:1–19:30, Aug. 2009.
- [21] S. T. Le, K. Schuh, F. Buchali, and H. Buelow, "100 Gbps b-modulated Nonlinear Frequency Division Multiplexed Transmission," in *2018 Optical Fiber Communications Conference and Exposition (OFC)*, March 2018, pp. 1–3.
- [22] E. H.-L. Liu, "Fundamental Methods of Numerical Extrapolation with Applications," MIT open courseware, Massachusetts Institute of Technology, 2006, accessed: 1-11-2018. [Online]. Available: <http://web.mit.edu/ehliu/Public/Spring2006/18.304/extrapolation.pdf>
- [23] J. McNamee and V. Y. Pan, "Efficient Polynomial Root-refiners: A Survey and New Record Efficiency Estimates," *Computers & Mathematics with Applications*, vol. 63, no. 1, pp. 239 – 254, 2012.
- [24] A. R. Osborne, "Nonlinear Fourier Methods for Ocean Waves," *Procedia IUTAM*, vol. 26, pp. 112–123, 2018.
- [25] E. V. Podivilov, D. A. Shapiro, and D. A. Trubitsyn, "Exactly Solvable Profiles of Quasi-rectangular Bragg Filter with Dispersion Compensation," *Journal of Optics A: Pure and Applied Optics*, vol. 8, no. 9, p. 788, 2006.
- [26] P. J. Prins and S. Wahls, "Higher Order Exponential Splittings for the Fast Non-Linear Fourier Transform of the Korteweg-de Vries Equation,"

- in *2018 IEEE International Conference on Acoustics, Speech, and Signal Processing (ICASSP)*, April 2018.
- [27] L. Rabiner, R. Schafer, and C. Rader, "The chirp z-transform algorithm," *IEEE Transactions on Audio and Electroacoustics*, vol. 17, no. 2, pp. 86–92, June 1969.
 - [28] D. Rourke and P. Morris, "Half-Solitons as Solutions to the Zakharov-Shabat Eigenvalue Problem for Rational Reflection Coefficient with Application in the Design of Selective Pulses in Nuclear Magnetic Resonance," *Phys. Rev. A*, vol. 46, no. 7, pp. 3631–3636, 1992.
 - [29] J. Satsuma and N. Yajima, "B. Initial Value Problems of One-Dimensional Self-Modulation of Nonlinear Waves in Dispersive Media," *Progress of Theoretical Physics Supplement*, vol. 55, pp. 284–306, 1974.
 - [30] A. Sidi, *Practical Extrapolation Methods: Theory and Applications*, 1st ed. New York, NY, USA: Cambridge University Press, 2002.
 - [31] A. C. Singer, A. V. Oppenheim, and G. W. Wornell, "Detection and Estimation of Multiplexed Soliton Signals," *IEEE Transactions on Signal Processing*, vol. 47, no. 10, pp. 2768–2782, Oct 1999.
 - [32] O. V. Sinkin, R. Holzlohner, J. Zweck, and C. R. Menyuk, "Optimization of the Split-step Fourier Method in Modeling Optical-fiber Communications Systems," *Journal of Lightwave Technology*, vol. 21, no. 1, pp. 61–68, Jan 2003.
 - [33] I. H. Sloan, *Superconvergence*. Boston, MA: Springer US, 1990, pp. 35–70.
 - [34] M. Thalhammer, "A Fourth-order Commutator-free Exponential Integrator for Nonautonomous Differential Equations," *SIAM Journal on Numerical Analysis*, vol. 44, no. 2, pp. 851–864, 2006. [Online]. Available: <https://doi.org/10.1137/05063042>
 - [35] S. K. Turitsyn *et al.*, "Nonlinear Fourier Transform for Optical Data Processing and Transmission: Advances and Perspectives," *Optica*, vol. 4, no. 3, pp. 307–322, Mar 2017.
 - [36] V. Vaibhav, "Higher Order Convergent Fast Nonlinear Fourier Transform," *IEEE Photonics Technology Letters*, vol. 30, no. 8, pp. 700–703, April 2018.
 - [37] A. Vasylichenkova, J. Prilepsky, D. Shepelsky, and A. Chattopadhyay, "Direct Nonlinear Fourier Transform Algorithms for the Computation of Solitonic Spectra in Focusing Nonlinear Schrödinger Equation," *Communications in Nonlinear Science and Numerical Simulation*, vol. 68, pp. 347 – 371, 2019.
 - [38] A. Vasylichenkova, J. E. Prilepsky, and S. K. Turitsyn, "Contour Integrals for Numerical Computation of Discrete Eigenvalues in the Zakharov&Shabat Problem," *Opt. Lett.*, vol. 43, no. 15, pp. 3690–3693, Aug 2018.
 - [39] S. Wahls, "Generation of Time-limited Signals in the Nonlinear Fourier Domain via b-Modulation," in *2017 European Conference on Optical Communication (ECOC)*, Sept 2017, pp. 1–3.
 - [40] S. Wahls, S. Chimmalgi, and P. Prins, "FNFT: A Software Library for Computing Nonlinear Fourier Transforms," *The Journal of Open Source Software*, vol. 3, p. 597, 2018.
 - [41] S. Wahls and H. V. Poor, "Introducing the Fast Nonlinear Fourier Transform," in *2013 IEEE International Conference on Acoustics, Speech and Signal Processing*, May 2013, pp. 5780–5784.
 - [42] —, "Fast Numerical Nonlinear Fourier Transforms," *IEEE Transactions on Information Theory*, vol. 61, no. 12, pp. 6957–6974, Dec 2015.
 - [43] M. Yamada and K. Sakuda, "Analysis of Almost-periodic Distributed Feedback Slab Waveguides via a Fundamental Matrix Approach," *Appl. Opt.*, vol. 26, no. 16, pp. 3474–3478, Aug 1987.
 - [44] M. I. Yousefi and F. R. Kschischang, "Information Transmission Using the Nonlinear Fourier Transform, Part I: Mathematical Tools," *IEEE Transactions on Information Theory*, vol. 60, no. 7, pp. 4312–4328, July 2014.
 - [45] —, "Information Transmission Using the Nonlinear Fourier Transform, Part II: Numerical Methods," *IEEE Transactions on Information Theory*, vol. 60, no. 7, pp. 4329–4345, July 2014.
 - [46] V. Zakharov and A. Shabat, "Exact Theory of Two-Dimensional Self-Focusing and One-Dimensional Self-Modulation of Waves in Nonlinear Media," *Soviet Physics JETP*, vol. 34, no. 1, p. 62, January 1972.